Paper

Int'l J. of Aeronautical & Space Sci. 18(2), 245–254 (2017)
DOI: doi.org/10.5139/IJASS.2017.18.2.245

IJASS
International Journal of Aeronautical and Space Sciences

Deployment Dynamics of Large-Scale Flexible Solar Arrays with Deployable Mast

Hai-Quan LI*, Xiao-Feng LIU, Shao-Jing GUO***, and Guo-Ping CAI******

Shanghai Jiao Tong University, Shanghai 200240, China

Abstract

In this paper, deployment dynamics of large-scale flexible solar arrays with deployable mast is investigated. The adopted solar array system is introduced firstly, then kinematic description and kinematic constraint equations are deduced, and finally, dynamics equation of the system is established by the Jourdain velocity variation principle and a new method to deal with topology changes of the deployable mast is introduced. The dynamic behavior of the system is studied in detail. Simulation results indicate that the proposed model is effective to describe the deployment dynamics of the solar arrays and that the introduced method is applicable for topology changes.

Key words: Solar array system, Dynamic modeling, Topology changes, Deployable mast

1. Introduction

Solar array system is one of the essential components of spacecraft. It provides power for the spacecraft in on-orbit flight. As more advanced missions are posed to spacecrafts and as higher performances are required of mission instruments, more electric power is required for spacecrafts to generate. Despite a trend toward greater diversity in the spacecraft class, an upper limit of electric power demand has increased steadily. To accommodate this requirement, larger solar array paddles have been developed [1,2] With the advent of large and light-weight solar arrays in spacecrafts, the flexibility of these arrays has become a concern since undesirable vibrations of these components could disrupt the mission of the spacecraft [3].

Deployable masts are frequently used in various space programs as basic structural members [4-7], and they are classified into two categories due to the ways of stowage [6]. One is a coilable longeron extendible mast, which is stowed through the coilable deformation of continuous elastic longerons, and another is an articulated one. Generally speaking, the latter shows stiffer mechanical properties for heavy duties, but it consists of a larger number of mechanism parts, which sometimes decrease deployment reliability. In the design and numerical simulation of articulated extendible mast systems for present and future space applications, reliability of deployment mechanisms and applicable dynamic modelling methods are strongly requested.

In recent years, the researches of solar arrays and deployable mast have attracted more and more attention, and considerable theoretical researches and engineering experiments have been done. For example, Loh [8] built a finite element model of prestressed solar arrays in structural dynamics and analyzed the effects of geometric stiffness on natural frequencies. Iwata, Fujii et al. [9] described a design optimization for a large solar array paddle deployment with various practical constraints and presented ground verification results. Yang [4] established a dynamic model of coilable mast and rigid solar arrays based on the multibody dynamic solver Thudynamics and revealed the parameter sensitivity that influences the reliability of coilable mast deployment. Laible, Fitzpatrick et al. [10] performed a detailed nonlinear analysis on the 2A array model to assess possible solutions to modal differences, and their study revealed that the array attachment structure is nonlinear and thus was the source

* Ph. D Student
** Ph. D Student
*** Ph. D Student
**** Professor, Corresponding author: caigp@sjtu.edu.cn

Received: June 23, 2016 Revised: May 23, 2017 Accepted: June 7, 2017

http://ijass.org pISSN: 2093-274x eISSN: 2093-2480

of error in the model prediction of mast modes. Shan et al. [5] designed a triangular prism modular deployable mast and analyzed kinematics behavior of the mast. From the researches above it can be seen that solar arrays and deployable mast have gained many attentions and many research results have been achieved. However, most of the researches focused on the deployed state of the solar arrays and researches about the deployable mast just studied the kinematics of the deployment and the force analysis of the mast on the deployed state; little attention has been paid to the deployment process of the mast with flexible solar arrays. Even in the very small amount of studies about deployment dynamics of solar arrays, the flexibility of sub-panels was not considered [4,9].

The solar arrays are deployed by the combined effects of the deployable mast, guy-wire and tension control mechanism. The deployment will affect the position and attitude of the spacecraft. Therefore, it is necessary to establish a dynamic model to analyse the deployment dynamics of the solar array system.

In this paper, deployment dynamics of large-scale flexible solar arrays is investigated. Dynamics modeling for the system is given and numerical simulations are done to reveal the system characteristics. This paper is organized as follows. Section 2 introduces the structure of the solar array system, including spacecraft main-body, deployable mast, latch mechanisms, drive mechanism, solar arrays, tension control mechanism, guy-wire and joint damper between sub-panels. In Section 3, dynamic equation of the solar array system is established by the Jourdain velocity variation principle and a method for dynamics with topology changes is introduced. Section 4 presents numerical simulations to validate the theoretical studies in this paper. Finally, a concluding remark is given in Section 5.

2. Solar array system with deployable mast

In this section, the structure of the solar array system adopted in this paper is firstly introduced (Fig. 1), then the latch mechanism and the limit spring of the deployable mast are studied, and finally the tension control mechanism, the guy-wires and the joint damper are discussed.

2.1 Deployable Mast

Deployable mast emerged with the development of aerospace exploring technology [6]. It is mainly used for extending flexible solar array and supporting deployable antenna, synthetic aperture radar and space telescope. Tubular boom, telescopic mast, coilable mast and some articulated masts have been developed and applied in outer space. In this paper, a triangular prism modular mast [5,11] as shown in Fig. 2 is adopted.

Figure 2 shows the triangular prism modular deployable mast. Three screws are installed outside each node of triangular frames. Each frame can be held in turn by the screw driving the rollers on three corners of the frame. The rollers contain one rotational degree of freedom which is beneficial for decreasing frictions between screws and rollers. There are limiting springs [11] (Fig. 3) so that the latter unit will not be held until the former unit is fully deployed. This sequence

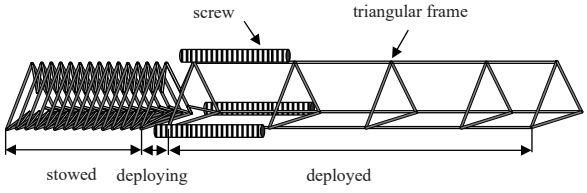

Fig. 2. The deployable mast

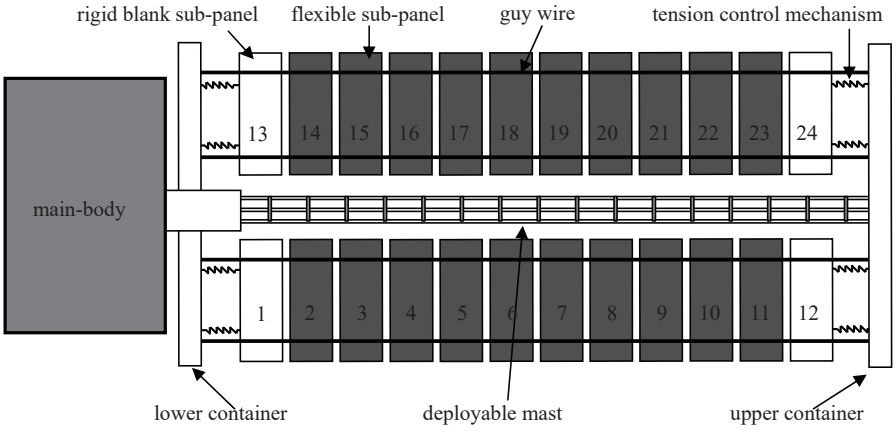

Fig. 1. The solar array system

repeats until the whole mast is deployed.

2.2 Solar Arrays

As shown in Fig. 1. The solar arrays consist of rigid and flexible sub-panels, two containers, four guy-wires and the tension control mechanism. The lower container is fixed on the spacecraft mainbody. The deployable mast drives the upper container, and the upper container pulls the sub-panels by ropes of the tension control mechanism to complete the deployment.

The tension control mechanism (TCM) is designed to provide tensional force to the sub-panels. The purpose of this force is to keep the sub-panel stiff [12]. In this paper, the tension control mechanism is simplified as a spring and a damper when the rope is stretched (Fig. 4), and there is no tensional force when the rope is not stretched. The tensional force can be written as

$$F_{\text{tcm}} = \begin{cases} -k_{\text{tcm}} \times \delta l_{\text{tcm}} - c_{\text{tcm}} \times \delta v_{\text{tcm}}, & \delta l_{\text{tcm}} > 0 \\ 0, & \delta l_{\text{tcm}} \le 0 \end{cases} \tag{1}$$

where k_{tcm} is the stiffness, c_{tcm} is the damping coefficient, δv_{tcm} is the relative velocity between the container and the blank rigid sub-panel and δv_{tcm} is the stretched length of the rope.

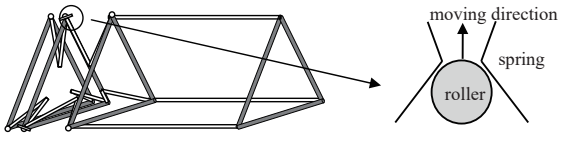

Fig. 3. The limiting springs

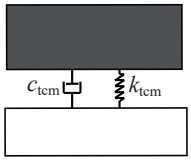

Fig. 4. Tension control mechanism (TCM)

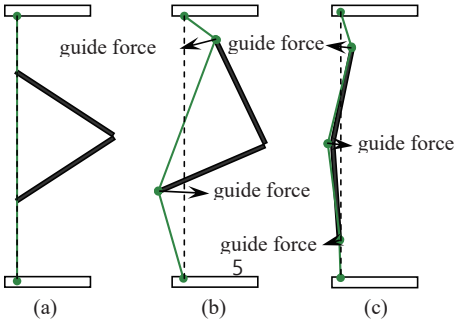

Fig. 5. Schematic diagram of guy-wire: (a) normal state, (b) large deviation, (c) reverse folding

As shown in Figs. 1, there are four guy-wires to keep the sub-panels from large deviation or reverse folding state [4]. When the sub-panels are deployed with normal state, there is no force acting on the sub-panels by the guy-wire (Fig. 5 (a)); when large deviation (Fig. 5 (b)) or reverse folding state (Fig.5 (c)) occur, tension of the guy-wire acts on the sub-panels to pull them back to the normal state.

The sub-panels are connected by revolution joints with damping, when the deployment is completed, the joint will reach its final position with some momentum that will result in overshoot and oscillation. The extinguishing of that oscillation is the purpose of a damper [13]. The damping torque can be calculated as

$$T_{\text{joint}} = -c_{\text{joint}} \times \omega_{\text{joint}} \tag{2}$$

where c_{joint} is the damping coefficient of the joint and ω_{joint} is the angular velocity of the joint.

3 Dynamic Model of the System

In this section, the kinematic description of an arbitrary point on a flexible body is deduced firstly, then kinematic constraint of a pair of bodies is presented, subsequently the dynamic equation of a single flexible body is established using the Jourdain velocity variation principle and the dynamic equation of constrained multibody system is formulated by the augmented method, finally a simple and accurate method based on the impulse–momentum equation for the numerical simulation of multi-body systems with topology changes is introduced.

3.1 Kinematic Description of Flexible Body

For an arbitrary flexible body in the multibody system, the deformation of each point is expressed in terms of a finite number of coordinates [14]

$$\boldsymbol{u}' = \boldsymbol{\Phi a} \tag{3}$$

where $\boldsymbol{\Phi}=(\boldsymbol{\phi}_1 \cdots \boldsymbol{\phi}_s)$, $\boldsymbol{a}=(a_1 \cdots a_s)^T$ and $a_m\,(m=1, \ldots, s)$ is the m-th modal coordinate, $\boldsymbol{\phi}_m\,(m=1, \ldots, s)$ is the corresponding vector

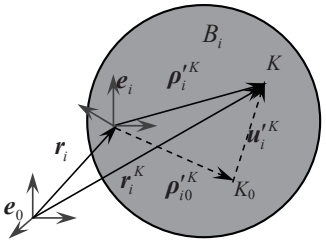

Fig. 6. Schematic diagram of a flexible body

of mode function and *s* mean that that the first s models are chosen.

As shown in Fig. 6, for an arbitrary flexible body B_i in the system, we select a body reference $\boldsymbol{e}_i$ whose location and orientation with respect to the global coordinate system $\boldsymbol{e}_0$ are defined by a set of coordinates called reference coordinates and denoted as $\boldsymbol{q}_{ri}$, the vector $\boldsymbol{q}_{ri}$ can be written in a partitioned form as

$$\boldsymbol{q}_{ri} = [\boldsymbol{r}_i^{\mathrm{T}} \quad \boldsymbol{\Lambda}_i^{\mathrm{T}}]^{\mathrm{T}} \tag{4}$$

where $\boldsymbol{r}_i$ is a set of Cartesian coordinates that define the location of the origin of the body reference $\boldsymbol{e}_i$ and $\boldsymbol{\Lambda}_i=[\Lambda_0 \ \Lambda_1 \ \Lambda_2 \ \Lambda_3]_i^{\mathrm{T}}$ is a set of the four Euler parameters that describe the orientation of the selected body reference [14], the superscript T represents the transpose of a matrix or vector.

The global position of an arbitrary point K on the rigid body can be written as

$$\boldsymbol{r}_i^K = \boldsymbol{r}_i + \boldsymbol{\rho}_i^K = \boldsymbol{r}_i + 2\boldsymbol{R}_i\boldsymbol{L}_i^{\mathrm{T}}\boldsymbol{\rho}_i'^K \tag{5}$$

where $\boldsymbol{R}_i$ and $\boldsymbol{L}_i$ are defined as functions of the four Euler parameters [16].
and the vector $\boldsymbol{\rho}_i'^K$ can be written as

$$\boldsymbol{\rho}_i'^K = \boldsymbol{\rho}_{i0}'^K + \boldsymbol{u}_i'^K = \boldsymbol{\rho}_{i0}'^K + \boldsymbol{\Phi}_i^K\boldsymbol{a}_i \tag{6}$$

where $\boldsymbol{\rho}_{i0}^K$ is the position of the point *K* in the undeformed state, $\boldsymbol{\Phi}_i^K$ is the corresponding matrix of mode function and $\boldsymbol{a}_i$ is the modal coordinate vector of the flexible body B_i. $\boldsymbol{\Phi}_i^K$ is a constant matrix which could be obtained using the finite element program NASTRAN [10]. One can then write the global position of the point *K* on the body B_i as

$$\boldsymbol{r}_i^K = \boldsymbol{r}_i + \boldsymbol{\rho}_i^K = \boldsymbol{r}_i + 2\boldsymbol{R}_i\boldsymbol{L}_i^{\mathrm{T}}(\boldsymbol{\rho}_{i0}'^K + \boldsymbol{\Phi}_i^K\boldsymbol{a}_i) \tag{7}$$

in which the global position of the point *K* is written in terms of the generalized reference and modal coordinates of the body B_i. Therefore, we define the coordinates of the body B_i as

$$\boldsymbol{q}_i = [\boldsymbol{r}_i^{\mathrm{T}} \quad \boldsymbol{\Lambda}_i^{\mathrm{T}} \quad \boldsymbol{a}_i^{\mathrm{T}}]^{\mathrm{T}} \tag{8}$$

Differentiating Eq. (7) with respect to time yields

$$\dot{\boldsymbol{r}}_i^K = \dot{\boldsymbol{r}}_i - 2\tilde{\boldsymbol{\rho}}_i^K\boldsymbol{R}_i\dot{\boldsymbol{\Lambda}}_i + 2\boldsymbol{R}_i\boldsymbol{L}_i^{\mathrm{T}}\boldsymbol{\Phi}_i^K\dot{\boldsymbol{a}}_i \tag{9}$$

where "˙" denotes differentiation with respect to time. Since $\boldsymbol{\rho}_i^K$ is the position of the point *K* in the deformed state that can be written as $\boldsymbol{\rho}_i^K = [\rho_{i1}^K \quad \rho_{i2}^K \quad \rho_{i3}^K]^{\mathrm{T}}$, throughout the text the symbol "~" denotes a skew symmetric matrix, $\tilde{\boldsymbol{\rho}}_i^K$ in Eq. (9) is defined as [15]

$$\tilde{\boldsymbol{\rho}}_i^K = \begin{bmatrix} 0 & -\rho_{i3}^K & \rho_{i2}^K \\ \rho_{i3}^K & 0 & -\rho_{i1}^K \\ -\rho_{i2}^K & \rho_{i1}^K & 0 \end{bmatrix} \tag{10}$$

The acceleration of the point *K* can be determined by direct differentiation of Eq. (9). This leads to

$$\ddot{\boldsymbol{r}}_i^K = \ddot{\boldsymbol{r}}_i - 2\tilde{\boldsymbol{\rho}}_i^K\boldsymbol{R}_i\ddot{\boldsymbol{\Lambda}}_i + 2\boldsymbol{R}_i\boldsymbol{L}_i^{\mathrm{T}}\boldsymbol{\Phi}_i^K\ddot{\boldsymbol{a}}_i + 4\tilde{\boldsymbol{\omega}}_i\boldsymbol{R}_i\boldsymbol{L}_i^{\mathrm{T}}\boldsymbol{\Phi}_i^K\dot{\boldsymbol{a}}_i + \tilde{\boldsymbol{\omega}}_i\tilde{\boldsymbol{\omega}}_i\boldsymbol{\rho}_i^K \tag{11}$$

where $\boldsymbol{\omega}_i = 2\boldsymbol{R}_i\dot{\boldsymbol{\Lambda}}_i$ is the angular velocity of the body B_i.

Equations (9) and (3) can be written in the following matrix form

$$\dot{\boldsymbol{r}}_i^K = \boldsymbol{B}_i^K\dot{\boldsymbol{q}}_i \tag{12}$$

$$\ddot{\boldsymbol{r}}_i^K = \boldsymbol{B}_i^K\ddot{\boldsymbol{q}}_i + \boldsymbol{w}_i^K \tag{13}$$

where $\boldsymbol{B}_i^K = (\boldsymbol{I}_3 \quad -2\tilde{\boldsymbol{\rho}}_i^K\boldsymbol{R}_i \quad 2\boldsymbol{R}_i\boldsymbol{L}_i^{\mathrm{T}}\boldsymbol{\Phi}_i^K)$ and $\boldsymbol{w}_i^K = 4\tilde{\boldsymbol{\omega}}_i\boldsymbol{R}_i\boldsymbol{L}_i^{\mathrm{T}}\boldsymbol{\Phi}_i^K\dot{\boldsymbol{a}}_i + \tilde{\boldsymbol{\omega}}_i\tilde{\boldsymbol{\omega}}_i\boldsymbol{\rho}_i^K$; the matrices $\dot{\boldsymbol{q}}_i = [\dot{\boldsymbol{r}}_i^{\mathrm{T}} \quad \dot{\boldsymbol{\Lambda}}_i^{\mathrm{T}} \quad \dot{\boldsymbol{a}}_i^{\mathrm{T}}]^{\mathrm{T}}$ and $\dot{\boldsymbol{q}}_i = [\ddot{\boldsymbol{r}}_i^{\mathrm{T}} \quad \ddot{\boldsymbol{\Lambda}}_i^{\mathrm{T}} \quad \ddot{\boldsymbol{a}}_i^{\mathrm{T}}]^{\mathrm{T}}$ are the total vectors of generalized velocity and generalized acceleration of the body B_i, respectively.

3.2 Kinematic Constraints

The kinematic constraint equations of the system can be written as

$$\boldsymbol{C}_\alpha\boldsymbol{q}_\alpha + \boldsymbol{C}_\beta\boldsymbol{q}_\beta = \boldsymbol{0} \tag{14}$$

where the subscript α and β define the two bodies connected by the joint.

Taking the second derivative of Eq. (6), we have

$$\boldsymbol{C}_{q_\alpha}\ddot{\boldsymbol{q}}_\alpha + \boldsymbol{C}_{q_\beta}\ddot{\boldsymbol{q}}_\beta = \boldsymbol{\gamma} \tag{15}$$

where $\boldsymbol{C}_{qi} = \dfrac{\partial \boldsymbol{C}}{\partial \boldsymbol{q}_i}(i = \alpha, \beta)$ is the constraint Jacobian matrix of the body $B_i(i=\alpha, \beta)$, the symbol ∂ is the partial derivative operator and the right term of Eq. (7) is

$$\boldsymbol{\gamma} = -\boldsymbol{C}_{tt} - (\boldsymbol{C}_q\dot{\boldsymbol{q}})_q\dot{\boldsymbol{q}} - 2\boldsymbol{C}_{qt}\boldsymbol{q} \tag{16}$$

where $\boldsymbol{C}_{tt} = \dfrac{\partial^2 \boldsymbol{C}}{\partial t^2}$ and $\boldsymbol{C}_{qt} = \dfrac{\partial^2 \boldsymbol{C}}{\partial t \partial \boldsymbol{q}}$.

Further more, the four Euler parameters satisfy the relation

$$C_i^{\Lambda} = \sum_{k=0}^{3}(\Lambda_k)_i^2 = \boldsymbol{\Lambda}_i^{\mathrm{T}}\boldsymbol{\Lambda}_i = 1, \ (i = \alpha, \beta) \tag{17}$$

Taking the second derivative of Eq. (9), we have

$$2\boldsymbol{\Lambda}_i^{\mathrm{T}}\ddot{\boldsymbol{\Lambda}}_i = -2\dot{\boldsymbol{\Lambda}}_i^{\mathrm{T}}\dot{\boldsymbol{\Lambda}}_i \tag{18}$$

Equations (7) and (10) will be used in the next section to build the augmented dynamics equation of the system.

3.3 Dynamics equation

Here we establish the dynamics equation of an arbitrary body B_i based on the Jourdain velocity variation principle

and assemble the dynamics equation of the system by the augmented method.

The lumped mass finite element method is used to divide the body B_i into l_e elements, and the mass of the body B_i is lumped to l nodes. According to the variation principle, the speed variation form of dynamic equation of the body B_i can be written as [16]

$$\sum_{K=1}^{l} \delta \ddot{\boldsymbol{r}}_i^{K\mathrm{T}} (-m_i^K \ddot{\boldsymbol{r}}_i^K + \boldsymbol{F}_i^K) - \delta \dot{\boldsymbol{a}}_i^{\mathrm{T}} (\boldsymbol{C}^{ai} \dot{\boldsymbol{a}}_i + \boldsymbol{K}^{ai} \dot{\boldsymbol{a}}_i) = 0 \tag{19}$$

where m_i^K is the lumped mass of the node K, $\boldsymbol{F}_i^k$ is the force acting on the node K, $\boldsymbol{C}^{ai}$ and $\boldsymbol{K}^{ai}$ are the modal damping and stiffness matrices of the body B_i.

With the use of Eqs. (4) and (5), Eq. (19) leads to

$$\delta \dot{\boldsymbol{q}}_i^{\mathrm{T}} (-\boldsymbol{M}_i \ddot{\boldsymbol{q}}_i - \boldsymbol{f}_i^{\mathrm{w}} + \boldsymbol{f}_i^{\mathrm{o}} - \boldsymbol{f}_i^{\mathrm{u}}) = 0 \tag{20}$$

where $\boldsymbol{M}_i$ is the generalized mass matrix of the body B_i; $\boldsymbol{f}_i^{\mathrm{o}}$, $\boldsymbol{f}_i^{\mathrm{w}}$ and $\boldsymbol{f}_i^{\mathrm{u}}$ are the vectors of generalized external force, generalized inertial force and generalized deformation force, respectively.

In this paper, the augmented method [14] is used to formulate the dynamics equation of constrained multibody systems. Considering the constraint force, dynamics equation of the system can be written as

$$\delta \dot{\boldsymbol{q}}^{\mathrm{T}} (\boldsymbol{M}\ddot{\boldsymbol{q}} - \boldsymbol{Q} + \boldsymbol{C}_{\boldsymbol{q}}^{\mathrm{T}} \boldsymbol{\lambda} + \boldsymbol{C}_{\boldsymbol{\Lambda}}^{\mathrm{T}} \boldsymbol{\lambda}_{\boldsymbol{\Lambda}}) = 0 \tag{21}$$

where $\boldsymbol{M} = \begin{bmatrix} \boldsymbol{M}_1 & & \\ & \ddots & \\ & & \boldsymbol{M}_{nb} \end{bmatrix}$, $\boldsymbol{C}_{\boldsymbol{\Lambda}} = \begin{bmatrix} (\boldsymbol{0} & \boldsymbol{\Lambda}_1^{\mathrm{T}}) & \\ & \ddots & \\ & & (\boldsymbol{0} \quad \boldsymbol{\Lambda}_{nb}^{\mathrm{T}}) \end{bmatrix}$,

$\boldsymbol{Q} = [\boldsymbol{Q}_1^{\mathrm{T}} \quad \cdots \quad \boldsymbol{Q}_{nb}^{\mathrm{T}}]^{\mathrm{T}}$ and $\boldsymbol{Q}_i = -\boldsymbol{f}_i^{\mathrm{w}} + \boldsymbol{f}_i^{\mathrm{o}} - \boldsymbol{f}_i^{\mathrm{u}}$, $(i = 1, \ldots, nb)$

The matrix $\boldsymbol{C}_{\boldsymbol{q}}$ in Eq. (21) is the constraint Jacobian matrix, $\boldsymbol{\lambda} = [\lambda_1 \quad \lambda_2 \quad \cdots \quad \lambda_{nc}]^{\mathrm{T}}$ is the vector of Lagrange multipliers, $\boldsymbol{\lambda}_{\boldsymbol{\Lambda}}$ is the Lagrange multiplier vector of the constraint equation (9) and $\boldsymbol{C}_{\boldsymbol{\Lambda}}$ is the constraint Jacobian matrix of the four Euler parameters.

Then the dynamics equation of the system can be written as [14]

$$\boldsymbol{M}\ddot{\boldsymbol{q}} - \boldsymbol{Q} + \boldsymbol{C}_{\boldsymbol{q}}^{\mathrm{T}} \boldsymbol{\lambda} + \boldsymbol{C}_{\boldsymbol{\Lambda}}^{\mathrm{T}} \boldsymbol{\lambda}_{\boldsymbol{\Lambda}} = \boldsymbol{0} \tag{22}$$

Equations (7), (10) and (22) can then be combined in one matrix equation as

$$\begin{bmatrix} \boldsymbol{M} & \boldsymbol{C}_{\boldsymbol{\Lambda}}^{\mathrm{T}} & \boldsymbol{C}_{\boldsymbol{q}}^{\mathrm{T}} \\ \boldsymbol{C}_{\boldsymbol{\Lambda}} & \boldsymbol{0} & \boldsymbol{0} \\ \boldsymbol{C}_{\boldsymbol{q}} & \boldsymbol{0} & \boldsymbol{0} \end{bmatrix} \begin{bmatrix} \ddot{\boldsymbol{q}} \\ \boldsymbol{\lambda}_{\boldsymbol{\Lambda}} \\ \boldsymbol{\lambda} \end{bmatrix} = \begin{bmatrix} \boldsymbol{Q} \\ \boldsymbol{\gamma}_{\boldsymbol{\Lambda}} \\ \boldsymbol{\gamma} \end{bmatrix} \tag{23}$$

where $\boldsymbol{\gamma}_{\boldsymbol{\Lambda}} = \begin{bmatrix} -\dot{\boldsymbol{\Lambda}}_1^{\mathrm{T}} \dot{\boldsymbol{\Lambda}}_1 \\ \vdots \\ -\dot{\boldsymbol{\Lambda}}_{nb}^{\mathrm{T}} \dot{\boldsymbol{\Lambda}}_{nb} \end{bmatrix}$.

Equation (23) is dynamics equation of the system that can be solved for the acceleration vector $\ddot{\boldsymbol{q}}$ and the vector of Lagrange multipliers. Given a set of initial conditions, the acceleration vector can be integrated to obtain the velocities and the generalized coordinates [16].

3.4 A Methodology for Topology Changes

The deployable mast is a common variable topology mechanism. Each deployable unit has three latch mechanisms. The latch mechanisms will cause changes of the degrees of freedom of the studied system, and calculations of many contacts will be introduced into the simulation.

A traditional method employs contact/impact mechanics in that the local contact/impact areas are modeled as spring-damping systems [17-19]. This method is suitable for understanding the effects of topology change events on the whole system. However, the time step must be limited to a small enough magnitude for the introduction of oscillation equations with a large stiffness term. The small time steps substantially increase the computational task, which makes it very difficult to simulate the deployment of the solar array system with many latch mechanisms.

Another class of methods is suitable for large temporal and super real-time simulations because the topology changes are modeled as instantaneous events that have relatively larger step sizes, which can be used for integration [20-25]. This method is suitable for the solar array system because the topology changes are modeled as instantaneous events that have relatively larger step size for integration.

In the second method, the topological changes, such as the locking or releasing of specific degrees of freedom and the formation or breaking of kinematic loops, are called "events" [25]. Let t^- and t^+ represent the beginning and ending moments of the adjustment; the duration of the progress can be expressed as $\Delta t = t^+ - t^-$, and $\Delta t \to 0$. For notational convenience, we use – and + to represent the start and end moments of an event, respectively. In this method, we consider that the generalized coordinates are invariant while the generalized velocities and accelerations are non-smooth when an event occurs:

$$\boldsymbol{q}(t) = \boldsymbol{q}^- = \boldsymbol{q}^+ = \overline{\boldsymbol{q}} = \text{const}, \quad t \in [t^-, t^+] \tag{24}$$

In this method, the following linear algebraic equations are obtained [20]:

$$\begin{bmatrix} \boldsymbol{M}(\overline{\boldsymbol{q}}) & \boldsymbol{C}_{after}^{\mathrm{T}}(\overline{\boldsymbol{q}}) \\ \boldsymbol{C}_{after}(\overline{\boldsymbol{q}}) & \boldsymbol{0} \end{bmatrix} \begin{bmatrix} \Delta \boldsymbol{v} \\ \boldsymbol{\mu} \end{bmatrix} = \begin{bmatrix} \boldsymbol{0} \\ -\boldsymbol{C}_{after}(\overline{\boldsymbol{q}}) \boldsymbol{v}^- \end{bmatrix} \tag{25}$$

Table 1. Parameters of the solar arrays

Item	Width	Thickness	Length	Mass	Inertia J_{xx}	Inertia J_{yy}	Inertia J_{zz}	Elasticity modulus
Unit	m	m	m	kg	kg·m^2	kg·m^2	kg·m^2	GPa
Value	2.4	7e-4	0.44	0.931	0.456	0.017	0.473	6

Table 2. Parameters of the triangular frame

Item	Length of side	Mass	Inertia J_{xx}	Inertia J_{yy}	Inertia J_{zz}
Unit	m	kg	kg·m^2	kg·m^2	kg·m^2
Value	0.3	0.19	1.29e-3	1.29e-3	2.57e-3

Table 3. Parameters of the deployable mast longeron

Item	Length	Mass	Inertia J_{xx}	Inertia J_{yy}	Inertia J_{zz}
Unit	m	kg	kg·m^2	kg·m^2	kg·m^2
Value	0.162	9.84e-2	2e-4	4.89e-6	2e-4

where $\boldsymbol{M}(\bar{\boldsymbol{q}})$ stands for the mass matrix, $\boldsymbol{C}_{after}(\bar{\boldsymbol{q}})$ is the Jacobian of the constraint equations after the occurrence of an event and $\boldsymbol{\mu}$ represents the impulsive constraint forces. Equation (25) can be solved for the change in the generalized velocities, and then the generalized velocities after an event can be calculated.

4. Numerical Simulation

In this section, the validity of the dynamic model proposed in this paper is verified firstly, and then simulations are conducted to analyze the dynamic behavior of the deployment. The solar array system is shown in Fig. 1, where 18 deployable units and 24 sub-panels are taken into account. The stiffness and damping of the tension control mechanism are chosen to be 200 N/m and 2N•s/m, respectively. The guide force of each guy-wire is chosen to be 10N, and the drive force is chosen to be 2000×(0.04 - v_T), where v_T is the velocity of the triangular frame of the deploying unit. Physical parameters of the system are given in Tables 1 - 3.

4.1 Verification of Dynamic Model

The validity of the dynamics modeling method proposed in this paper is verified through the comparison with ADAMS software. To simplify the simulation for comparison, a simple deployment model with eight sub-panels and six deployable units is considered, as shown in Fig. 7.

In this simulation, the local contact/impact areas are modeled as spring-damping systems. The lock torque is given by

$$T_{lock}(\theta_i) = step(\theta_i, x_1, 0, x_2, 1) \times bistop(\theta_i, \dot{\theta}_i, x_3, x_4, k_{bs}, e, c, d) \quad (26)$$

where

$$step(\theta_i, x_1, h_s^1, x_2, h_s^2) \quad (27)$$

$$= \begin{cases} h_s^1, & if\ \theta_i < x_1 \\ h_s^1 - (h_s^1 - h_s^2)\left(\dfrac{\theta_i - x_1}{x_2 - x_1}\right)^2 \left(3 - 2 \times \dfrac{\theta_i - x_1}{x_2 - x_1}\right), & if\ x_1 \le \theta_i \le x_2 \\ h_s^2, & if\ \theta_i > x_2 \end{cases}$$

and

$$bistop(\theta_i, \dot{\theta}_i, x_3, x_4, k_{bs}, e, c, d) \quad (28)$$

$$= \begin{cases} (k_{bs}(x_3 - \theta_i)^e - \dot{\theta}_i step(\theta_i, x_3 - d, c, x_3, 0), 0)_{\max}, & if\ \theta_i < x_3 \\ (-k_{bs}(\theta_i - x_4)^e - \dot{\theta}_i step(\theta_i, x_4, 0, x_4 + d, c), 0)_{\min}, & if\ \theta_i > x_4 \end{cases}$$

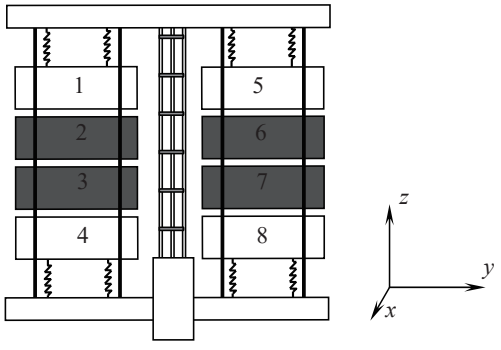

Fig. 7. Simplified solar array system

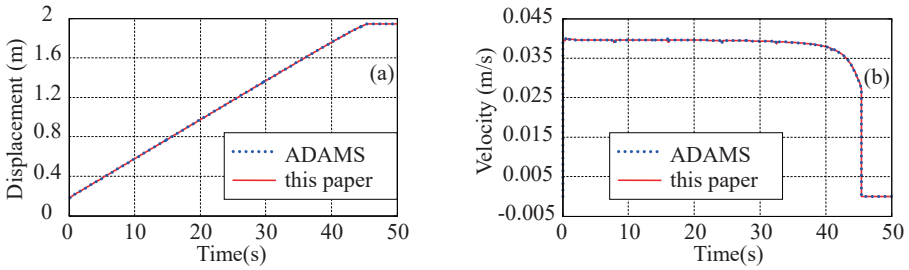

Fig. 8. Displacement and velocity of the upper container

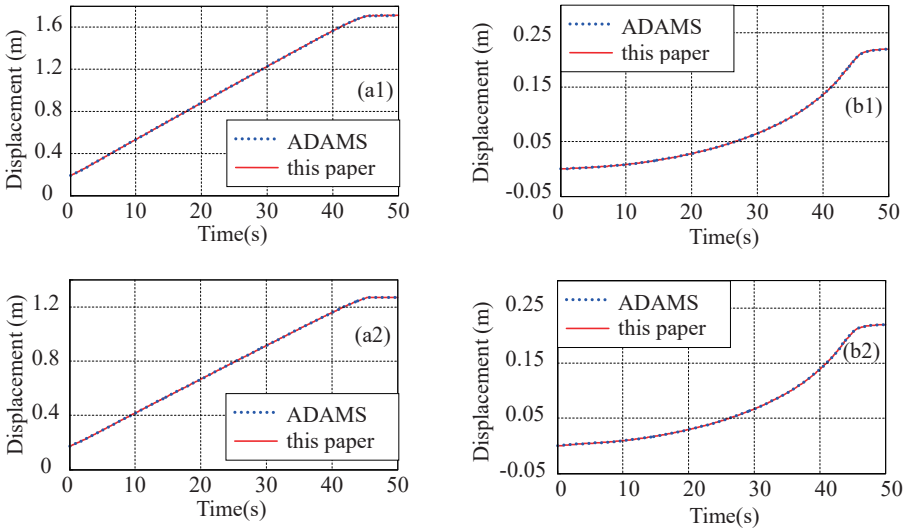

Fig. 9. Displacement of the sub-panels:(a) in x direction, (b) displacement in z direction

where $\dot{\theta}_i$ is the differential of θ_i, e is an exponent, k_{bs} is the equivalent stiffness, c is the damping coefficient and d is the distance depth.

The simulation results are presented in Figs. 8 and 9. These results show the displacements of the two panels during the deployment, where the solid line is the result using the proposed model and the dotted line using the ADAMS software. We can observe from Figs. 8 and 9 that the proposed model could achieve the same results as ADAMS software, which proves the validity of the proposed model.

4.2 Comparison of Different Methods

In this section, the simulations with different methods of the solar array system shown in Fig. 1 are conducted.

For the deployable mast, more and more joints of are locked during the deployment. There are too many spring and damping forces will be calculated in the simulation with the traditional method (Method 1). So the simulation

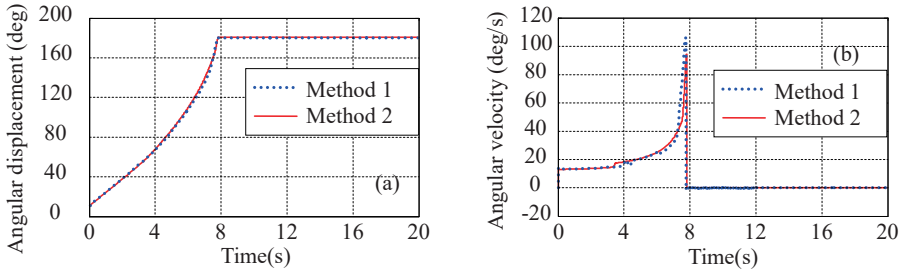

Fig. 10. Angular displacement and angular velocity of the deployable unit

will become very slow and divergence may occur. In this simulation, we compare the first 20 seconds of the deployment and the results are given in Fig. 10, where the dotted line is the result with the traditional method (Method 1) and the solid one is the result with the introduced method (Method 2).

It is observed from Fig. 10 that the simulation result with the new method introduced in this paper (Method 2) is similar to that of the simulation with the traditional method. This comparison also verified the conclusion of Guo and Wang [20]. So we can conclude that the introduced method could be used to describe complex dynamics problems with topology changes and that the calculation of a large number of spring-damping forces is avoided. So this method is more applicable for simulations of a long period of time than the spring-damping method.

4.3 Simulations with the Introduced Method

In this section, the simulation with the introduced method of the full-length solar array system shown in Fig. 1 is conducted. The parameters are given in Table 1. The 24 sub-panels are folded firstly and then deployed under the action of the deployable mast. After the deployment of the sub-panels is finished, the deployable mast continues to drive the upper container to stretch the tension control mechanism. We conduct the simulation from t=0s to t=150s in the following and the simulation results are given in Figs. 11 – 13.

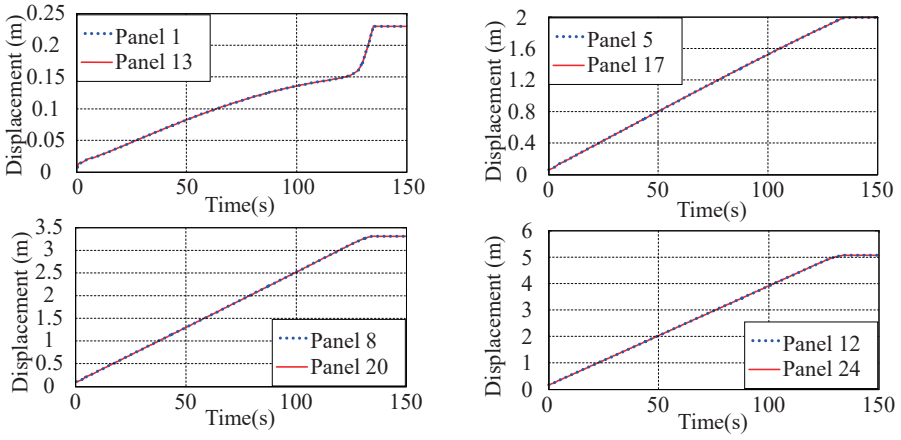

Fig. 11. Displacement of the sub-panels

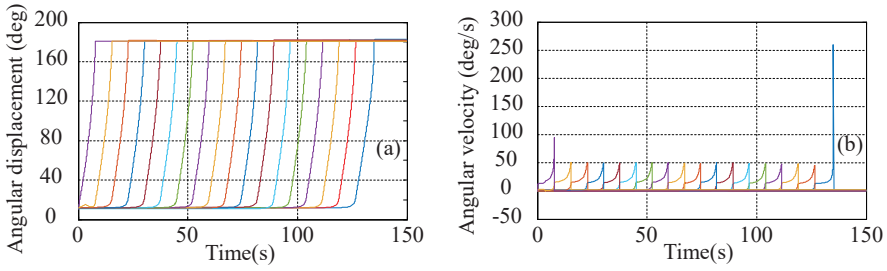

Fig. 12. Angular displacement and angular velocity of the deployable units

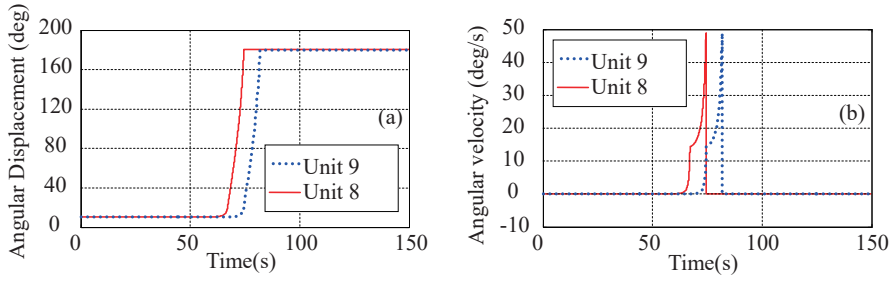

Fig. 13. Angular displacement and angular velocity of unit 8 and unit 9

Figure 11 shows the displacement of the sub-panels in the direction along the mast. From Fig. 11 we can see that the sub-panels are deployed smoothly and that the symmetrical sub-panels in the system have the same behavior during the deployment.

The angular displacement and angular velocity of the deployable units are given in Fig. 12. In order to analyze conveniently, the results of unit 8 and unit 9 are plotted in Fig. 13. From Fig. 13 we can see that the deployable units are deployed in proper order. Further more, discontinuous jumps of the angular velocity can be observed from Figs. 12b and 13b.

5. Conclusion

In this paper, deployment dynamics of a large-scale flexible solar array system with deployable mast is investigated. Dynamics equation of the solar array system is established by the Jourdain velocity variation principle and a new method is introduced for topology changes. Simulation results indicate that the proposed model is effective in describing the deployment dynamics of the large-scale flexible solar array system and that the introduced method is applicable for topology changes. The sudden transition in structural topology of the system could be simulated accurately and efficiently through the dynamics equation. The jumps in the generalized velocities when the topology changes occurred are calculated reasonably and precisely by the method introduced in this paper. The method captures the topology change explicitly by active and inactive aspects of the different constraint equation sets. Additionally, discontinuous jumps are calculated with the equations deduced from the integration of dynamics equation and velocity-level constraint violation equations.

Acknowledgement

This work is supported by the Natural Science Foundation of China (11132001, 11272202 and 11472171), the Key Scientific Project of Shanghai Municipal Education Commission (14ZZ021), the Natural Science Foundation of Shanghai (14ZR1421000) and Special Fund for Talent Development of Minhang District of Shanghai.

References

[1] Markelov, G. N. Kashkovsky, A. V. and Ivanov, M. S., "Space Station Mir Aerodynamics Along the Descent Trajectory", *Journal of Spacecraft and Rockets*, Vol. 38, No. 1, 2001, pp. 43-50.

[2] Riel, F. and Morata, L., "Space Station Freedom Pre-Integrated Truss Configuration", *AlAA Space Programs and Technologies Conference*, Huntsville, USA, 1992.

[3] Smith, S. and Mei, K., "Analytical Models for Nonlinear Responses of a Laboratory Solar Array", *The 38th Structures, Structural Dynamics, and Materials Conference*, Kissimmee, USA, 1997.

[4] Yang, J., "Multibody Dynamics of the Large-Scale Coilable Mast and Solar Array", M. Eng., Tsinghua University, 2013, in Chinese.

[5] Shan, M., Guo, H., Liu, R. and Wang, Y., "Design and Analysis of a Triangular Prism Modular Deployable Mast", *2013 IEEE International Conference*, Takamastu, Japan, 2013, pp. 1546-1551.

[6] Natori, M., Kitamura, T. and Kawamura, T., "Design of Articulated Extensible Mast Systems and Their Mechanical Characteristics", *The 37th Structures, Structural Dynamics and Materials Conference*, Salt Lake City, USA, 1996.

[7] Kitamura, T., Yamashiro, K., Obata, A. and Natori, M., "Development of a High Stiffness Extendible and Retractable Mast 'Himat' for Space Applications", *The 31st Structures, Structural Dynamics and Materials Conference*, Long Beach, USA, 1990.

[8] Loh, L., "Modeling of Prestressed Solar Arrays in Structural Dynamics", *Dynamics Specialists Conference*, Salt Lake City, USA, 1996.

[9] Iwata, T., Fujii, K. and Matsumoto, K., "Deployment Dynamics of a Large Solar Array Paddle", *AAS/AIAA Astrodynamics Specialist Conference*, Girdwood, USA, 2012.

[10] Laible M., Fitzpatrick K. and Grygier M., "International Space Station 2A Array Modal Analysis", *The 31st IMAC, A Conference on Structural Dynamics, Topics in Nonlinear Dynamic*s, Garden Grove, USA, 2013.

[11] Shan, M., "Mechanical Design and Analysis of A Triangular Prism Modular Deployable Mast", M. Eng., Harbin Institute of Technology, 2013, in Chinese.

[12] Kojima, Y., Taniwaki, S. and Ohkami, Y., "Attitude Vibration Caused by a Stick-Slip Motion for Flexible Solar Array of Advanced Earth Observation Satellite", *Journal of Vibration and Control*, Vol. 10, No. 10, 2004, pp. 1459-1472.

[13] Hinkley, D. and Simburger, E., "A Multifunctional Flexure Hinge for Deploying Omnidirectional Solar Arrays", *The 19th AIAA Applied Aerodynamics Conference*, Seattle, USA, 2001.

[14] Shabana, A. A., *Dynamics of Multibody Systems*, Cambridge University Press, 2005.

[15] Wittenburg, J., *Dynamics of Multibody Systems*, Springer Berlin Heidelberg, 2008.

[16] Hong, J. Z., *Computational Dynamics of Multibody*

Systems, Beijing: High Education Press, 1999, in Chinese.

[17] Gonthier, Y., McPhee, J., Lange, C. and Piedboeuf, J. C., "A Regularized Contact Model with Asymmetric Damping and Dwell-Time Dependent Friction", *Multibody System. Dynamics*, Vol. 11, No. 3, 2004, pp. 209-233.

[18] Shi, J., Hong, J. and Liu, Z., "Multi-Variable Approach of Contact-Impact Issue in Variable Topology System", *Theoretical and Applied Mechanics Letters*, Vol. 3, No. 1, 2013.

[19] Qi, F., Wang, T. and Li, J., "The Elastic Contact Influences on Passive Walking Gaits", *Robotica*, Vol. 29, No. 5, 2001, pp. 787-796.

[20] Guo, W. and Wang, T., "A Methodology for Simulations of Multi-rigid Body Systems with Topology Changes", *Multibody System Dynamics*, Vol. 35, No. 1, 2015, pp. 25-38.

[21] Wang, H., Eberhard, P. and Lin, Z., "Modeling and Simulation of Closed Loop Multibody Systems with Bodies-joints Composite Modules", *Multibody System Dynamics*, Vol. 24, No. 4, 2010, pp. 389-411.

[22] Glocker, C. and Pfeiffer, F., "Multiple Impacts with Friction in Rigid Multibody Systems", *Nonlinear Dynamics*, Vol. 7, No. 4, 1995, pp. 471-497.

[23] Mukherjee, R. M. and Anderson, K. S., "Efficient Methodology for Multibody Simulations with Discontinuous Changes in System Definition", *Multibody System Dynamics*, Vol. 18, No. 2, 2007, pp. 145-168.

[24] Khan, I., Poursina, M. and Anderson, K. S., "Model Transitions and Optimization Problem in Multi-flexible-body Systems: Application to Modeling Molecular Systems", *Computer Physics Communications*, Vol. 184, No. 7, 2013, pp. 1717-1728.

[25] Trinkle, J. C., Pang, J. S., Sudarsky, S. and Lo, G., "On Dynamic Multi-Rigid-Body Contact Problems with Coulomb Friction", *ZAMM-Journal of Applied Mathematics and Mechanics*, Vol. 77, No.4, 1997, pp. 267-279.